Journal of
Manufacturing and Materials Processing

MDPI

Communication

Dissimilar Welding of Thick Ferritic/Austenitic Steels Plates Using Two Simultaneous Laser Beams in a Single Pass

Fabio Giudice [1], Severino Missori [2] and Andrea Sili [3,*]

[1] Department of Civil Engineering and Architecture, University of Catania, 95123 Catania, Italy; fabio.giudice@unict.it
[2] Department of Industrial Engineering, University of Rome-Tor Vergata, 00133 Roma, Italy; missori@uniroma2.it
[3] Department of Engineering, University of Messina, 98166 Messina, Italy
* Correspondence: asili@unime.it

Abstract: Dissimilar welds between ferritic and austenitic stainless steels are widely used in industrial applications. Taking into account the issues inherent to arc welding, such as the high heat input and the need to carry out multiple passes in the case of thick plates, a procedure with two simultaneous laser beams (working in a single pass) and consumable inserts as filler metal has been considered. Particular attention was paid to the choice of the filler metal (composition and amount), as well as welding parameters, which are crucial to obtain the right dilution necessary for a correct chemical composition in the weld zone. The first experimental investigations confirmed the achievement of a good weldability of the dissimilar pair ASTM A387 ferritic/AISI 304L austenitic steel, having ascertained that the microstructure of the weld zone is austenitic with a little amount of residual primary ferrite, which is the best condition to minimize the risk of hot cracking.

Keywords: laser beam welding; dissimilar steels; consumable insert; dilution; weldability

Citation: Giudice, F.; Missori, S.; Sili, A. Dissimilar Welding of Thick Ferritic/Austenitic Steels Plates Using Two Simultaneous Laser Beams in a Single Pass. *J. Manuf. Mater. Process.* **2024**, *8*, 134. https://doi.org/10.3390/jmmp8040134

Academic Editor: Hui Huang

Received: 27 May 2024
Revised: 21 June 2024
Accepted: 24 June 2024
Published: 27 June 2024

1. Introduction

Dissimilar welds represent a satisfactory solution in many industrial applications to connect carbon or low-alloyed steel components with those made of an alloy best suited to elevated temperature service in corrosive environments. For stainless steel/carbon (or low-alloy) steel joining, a filler metal that is sufficiently alloyed to prevent martensitic microstructures in the fused zone (FZ) is highly desirable; otherwise, the precipitation of carbide and hardening phases [1] or the formation of martensitic microstructure [2] could occur in the FZ. In the case of thick components, it is necessary to carry out multi-pass arc welding, depositing the filler metal, layer by layer, into the weld groove; therefore, it produces at each pass reheating of the previous ones [3], as well as remelting and further dilution [4], which can affect the weld mechanical properties. With the purpose of obtaining sound bimetallic welds, many authors investigated the effects on the final microstructure of different filler metals [5] and V groove angles [6], as well as the advantage of the buttering technique, which prevents the formation of martensitic microstructure at the carbon steel side, as experimented by Asadollahi et al. [2]. These authors deposited a butter layer by GTAW before welding the dissimilar API 5L X65 ferritic and AISI 304L austenitic steels. For buttering, they used the ERNiCr3 Ni-based alloy, achieving positive results, since Ni diffusion towards the API ferritic steel decreases the Martensite start temperature and thus inhibits the formation of a brittle martensitic layer in the heat-affected zone, thus reducing the possibility of solidification cracking.

Furthermore, to limit carbon diffusion in the austenitic matrix and the consequent precipitation of Cr carbides (responsible for sensitizing intergranular corrosion), it is necessary to minimize the time spent at high temperatures [7]. However, this is not an achievable objective for arc welding, especially when performed by the multi-passing technique [8].

Nowadays, laser beam welding (LBW), due to the high level of energy concentrated in a small volume that allows one to weld thick plates with a single pass, has proven to be a suitable technology to obtain satisfactory joints between dissimilar metals, in general using wire filler metal [9].

The high energy density associated with the laser beam spot gives rise to a narrow plasma zone (the so-called "keyhole" mode), which in turn solidifies as a narrow and deep weld bead. Therefore, a proper choice of the welding parameters allows one to weld thick plates of AISI 304 stainless steel with a single pass and no filler metal [10]. In this case, the authors obtained an FZ microstructure characterized by columnar dendrites (growing from the interface to the center) and equiaxed dendrites in the center of the weld, with austenite as the major phase and δ-ferrite as the minor phase, whose formation can be ascribed to the high cooling rate during the non-equilibrium rapid solidification in deep penetration laser welding. For a comprehensive review of the effects of thermal gradient and composition, see the review of Nabavi et al. [11]; in particular the solidification mode of austenitic stainless steel depends on the ratio Cr_{eq}/N_{ieq}. When this parameter is in the range of 1.48–1.95, residual (skeletal and/or lathy) δ-ferrite remains in the microstructure due to the incomplete solid-state transformation from ferrite to austenite after solidification (FA solidification mode).

However, concerning dissimilar steels, the dilution between carbon steel and austenitic steel can lead, in the absence of a proper filler, to dangerous martensitic microstructures. In the case of LBW between AISI 1020 and AISI 304L thin sheets without filler metal, Scutelnico et al. [12] documented the formation of a hard martensitic microstructure in the FZ. Recently, Hamada et al. [13] carried out autogenous LBW between LA-UHSS low-alloy steel and AISI 316L austenitic stainless steel. Their metallographic investigation showed a martensitic microstructure in the FZ, due to supercooling, which enhances hardness.

For austenitic welds, it is well known that solidification as δ-ferrite (FA mode) gives the best resistance to weld solidification cracking [14]; a residual content above 5% of this phase is also desirable to prevent hydrogen embrittlement [15]. Unfortunately, concentrations of about 10% and above favor selective attack by some corrosive media; moreover, at temperatures in the 550–900 °C range, residual ferrite could decompose into carbides and phases detrimental for mechanical properties and corrosion resistance [16].

Another crucial aspect is represented by the correct balance between welding parameters, such as heat input and defocusing, to obtain satisfactory full penetration joints in thick steel plates [10].

To meet the best condition for FZ solidification and overcome the above-mentioned issues, the authors are currently working to carry out single-pass welding of dissimilar thick plates through an experimental setup with two simultaneous laser beams in an up-and-down configuration, each with a reduced heat input compared to the use of a single thermal source.

The object of this communication is to ascertain the weldability of two dissimilar ASTM A387 ferritic and AISI 304L austenitic steel plates, which were butt-positioned with two interposed consumable inserts to avoid the typical problems of feeding the filler wire.

The composition of the two filler metals and the welding parameters were chosen with the primary objective of obtaining molten pool conditions, such as to ensure the FA solidification mode, with a final microstructure consisting of austenitic dendrites with a low percentage of residual ferrite. Therefore, metallographic investigations were performed to ascertain the metallurgical features of the weldment and verify that the conditions for good weldability were achieved.

2. Materials and Methods

The welding trials were carried out using two simultaneous CO_2 gas laser beams (continuous wave, 0.5 mm focus diameter and zero defocusing distance with respect to the workpiece surface), which operated in robotic mode on two butt-positioned dissimilar plates (Figure 1).

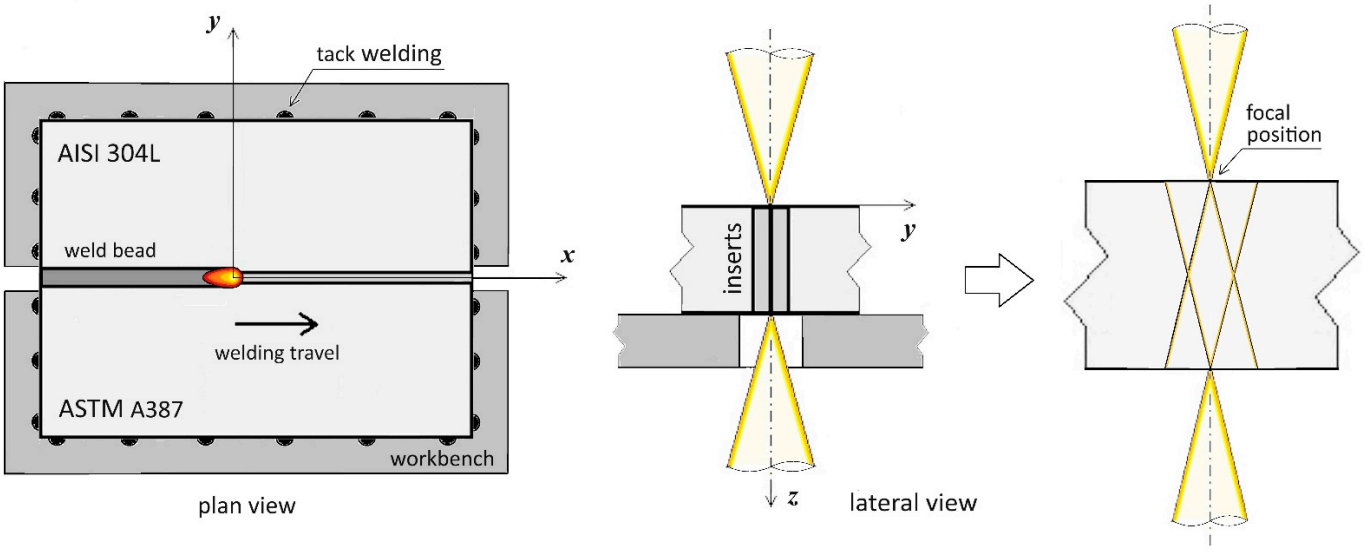

Figure 1. Sketch of the LBW setup and the interaction between the two laser beams (not in scale).

In general, the focal position plays an important role in the weld quality, determining the spot size, power density on the specimen surface and keyhole features; in [10], it was experimentally demonstrated that, for the same heat input, the welds obtained with a negative defocus are deeper than those with zero or positive defocus. However, their bottom surfaces are rough, owing to ejected spatters; conversely, at positive defocus, the bottom surface of the full penetration joints are smooth.

Based on these considerations, welding with two simultaneous lasers (United Technologies, East Hartford, CT, USA) represents an excellent choice to overcome the problems associated with the use of a single full penetration laser on thick plates. When welding with two simultaneous lasers, they work in less demanding conditions as the heat input of each is lower than what is necessary for a single thermal source. In this case, the FZ is the result of the effects of each laser, as shown in the sketch of Figure 1; therefore, a regular and symmetric shape can be expected.

The two plates (10 mm thick) were prepared with square edges, butt-positioned and placed horizontally (PA position for the upper laser beam and PE for the lower laser beam).

First, to hold the plates in place, tack-welding was performed manually by gas tungsten metal arc welding (GTMAW), using AWS ER 309L wire (diameter 0.8 mm) as the filler material (Fronius TIG welding machine, Wels, Austria). Punctual weld beads spaced approximately 20–25 cm all around their perimeter were obtained, taking care, on the short side, not to interfere with the consumable inserts.

Then, the two plates were treated with LBW in a single pass. Two different filler metals were added as consumable inserts interposed between the plates (each 0.5 mm wide, with 1.0 mm as their total width and A_F = 10 mm^2 as their total area in the yz plane) [17]. The following welding parameters were used: 10 kW power for each laser beam, 2.5 m/min (4.2 cm/s) welding speed and 2.38 kJ/cm heat input. The flow rate of helium, used as protective gas, was 25 L/min for each laser beam. The compositions of the two dissimilar base metals (BM1 and BM2) and the two filler metals (FM1 and FM2) are shown in Table 1.

Table 1. Parent metals and filler compositions (weight %).

	Standard	C	Mn	Si	P	S	Ni	Cr	Mo	Fe
Ferritic steel (BM1)	ASTM A387 Gr.22Cl.2	0.118	0.48	0.241	0.014	0.018	0.194	2.17	0.93	Bal.
Austenitic steel (BM2)	AISI 304L	0.018	1.15	0.41	0.025	0.001	10.1	18.4	-	Bal.
Weighted aver. composition ([1])		0.0915					2.82	6.47	0.68	Bal.
Filler metal (FM1)	EN X2CrNiMoN 22-8-3	0.013	1.66	0.48	0.029	0.015	23.1	8.7	3.14	Bal.
Filler metal (FM2)	EN X1CrNiMo 25-25-2	0.011	5.8	0.11	0.025	0.015	24.5	22.5	1.95	Bal.
Filler average composition ([2])		0.012					23.8	15.6	2.545	Bal.

([1]) EB = 0.735·BM1 + 0.265·BM2; ([2]) EF = (FM1 + FM2)/2.

Since the two base metals have similar latent heat of fusion (about 260–280 J/g) and different thermal conductivity (39 W/(m·K) for ferritic steel and 14 W/(m·K) for austenitic steel), their contribution to the formation of the molten zone is proportional to the value of the last parameter; therefore, a weighted average composition is reported in Table 1. The two consumable inserts were chosen to obtain a suitable composition in the FZ. By melting, they contribute equally to the FZ; therefore, their average composition is given in Table 1. The weld bead was investigated by visual inspections, macro- and micrographic optical observations of the cross-section and scanning electron microscopy with energy dispersive spectroscopy (SEM-EDS). For these observations, an Olimpus G71 optical microscope (Microscope System Limited, Glascow, UK) and a JEOL JSM-610F apparatus (JEOL Ltd., Tokyo, Japan) were used.

The micrographic observations were performed after suitable preparation by mechanical grinding and etching with the Glyceregia reagent (16% HNO_3, 42% HCl, 42% glycerol).

3. Results

Upon visual inspection, the weld bead shows a more regular shape than that which can be obtained with a single thermal source, without macroscopic cracks and defects, such as distortion, serious misalignments or undercuts (the jagged profile of the carbon steel near the FZ is due to chemical etching). The FZ profile, observed on different cross-sections, is essentially the same.

Figure 2a shows a representative macrograph of the FZ obtained with two simultaneous lasers, in which the full penetration along the whole thickness can be observed. The weld bead complies with all the requirements and recommendations on quality levels in steel laser beam-welded joints, according to ISO 13919-1:2019 [18]: internal imperfections (lack of fusion, cavities, incomplete penetration), surface imperfections (undercuts, weld metal excesses, toe overlap), and imperfections in joint geometry (linear misalignment) are minimal or absent. In particular, regarding the limit for undercuts and joint misalignments, the weld bead results in class B. Furthermore, it is characterized by a regular and symmetrical profile with an FZ width between 1.41 and 3.7 mm, greater than that of the inserts, demonstrating that the two base metals contributed to the formation of the joint.

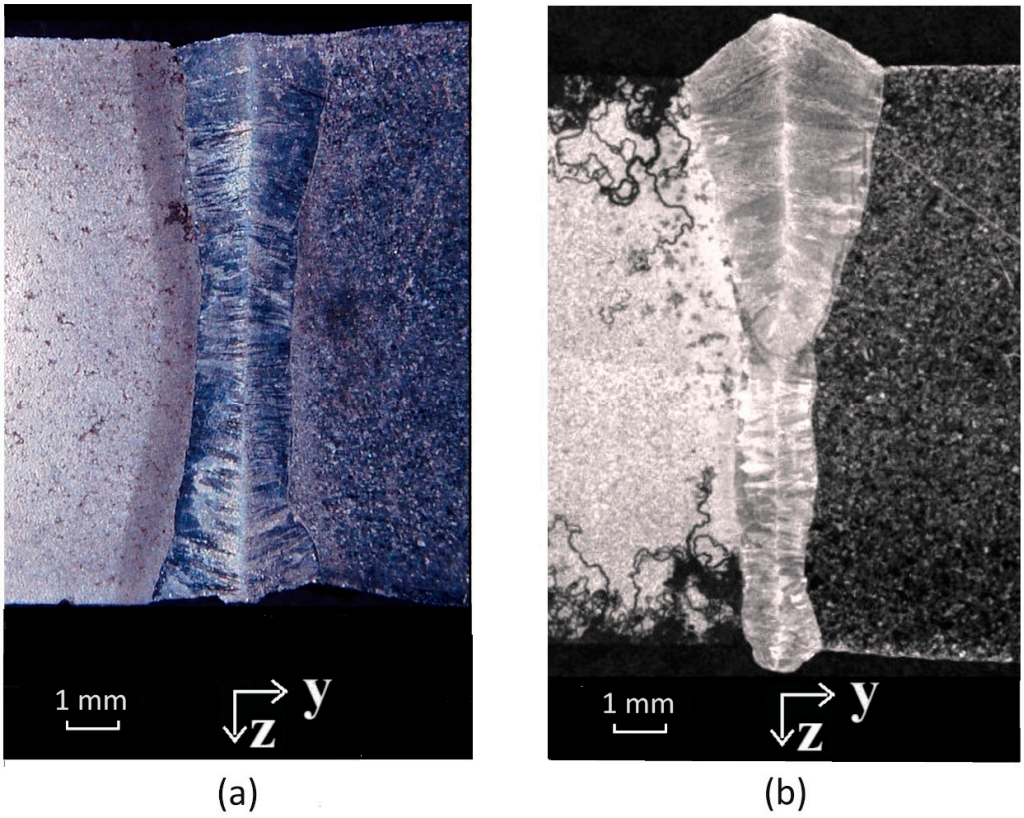

Figure 2. Macrographs of the FZ in comparison: (**a**) two simultaneous lasers (total heat input 4.76 kJ/cm); (**b**) single laser (heat input 5 kJ/cm).

For comparison, the FZ obtained with a single laser (having a heat input similar to the overall one of the two lasers) is shown in Figure 2b. Also in this case, full penetration is achieved; however, the weld bead quality is significantly lower than that shown in Figure 2a.

Metallographic investigations carried out on the weld obtained with two simultaneous lasers are shown in the following figures. The FZ microstructure is characterized by columnar dendrites which grow from the fusion lines (Figure 3) and converge towards the z axis (Figure 4).

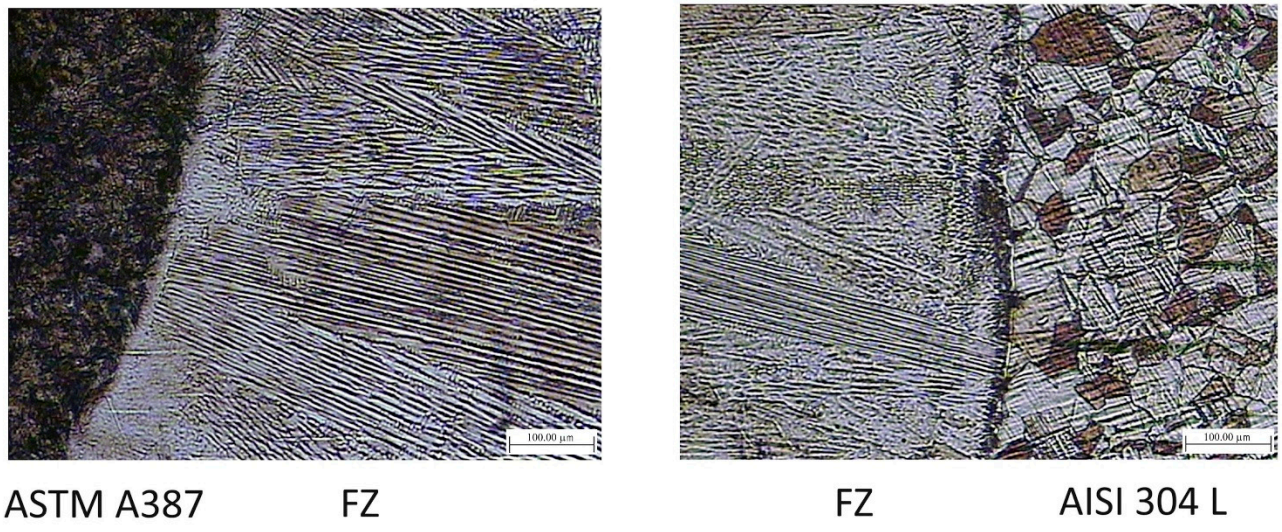

Figure 3. Weld macrograph of the FZ near the two parent metals.

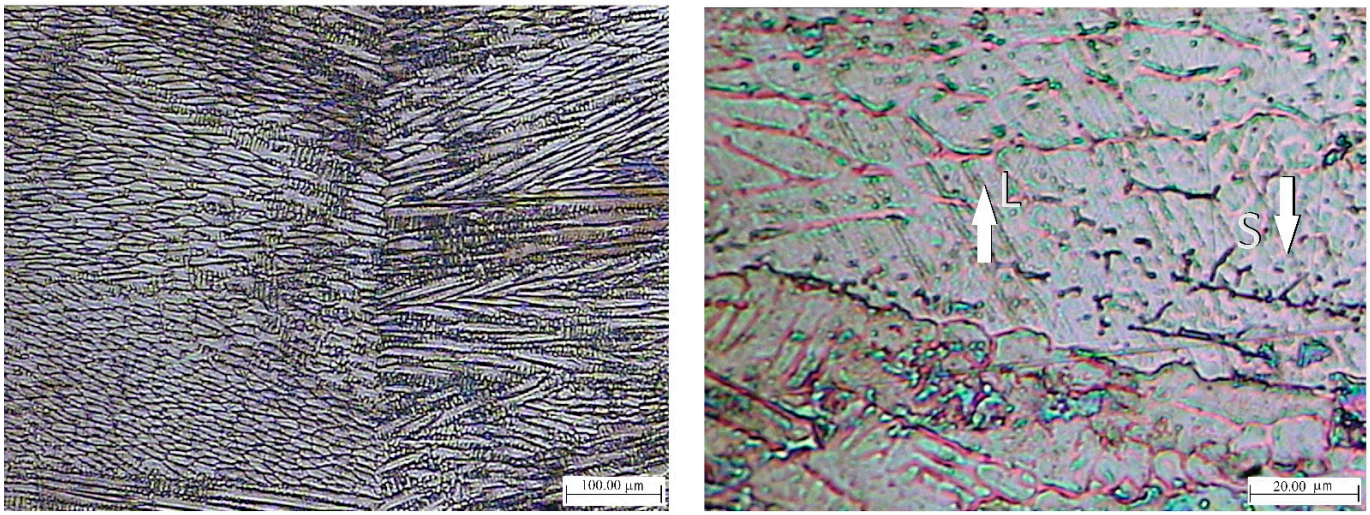

Figure 4. Micrograph of the FZ: (**a**) central area around the z axis; (**b**) detail with indication of lathy (L) and skeletal (S) δ-ferrite.

The FZ average composition resulting from the SEM-EDS microanalysis is given in Figure 5a, together with the image of the area where these measurements were performed; the line scans of Fe, Cr and Ni in Figure 5b show that the composition is constant across the FZ, with a sharp gradient at the boundary with the A387 parent metal, limiting the transition zone to a narrow strip.

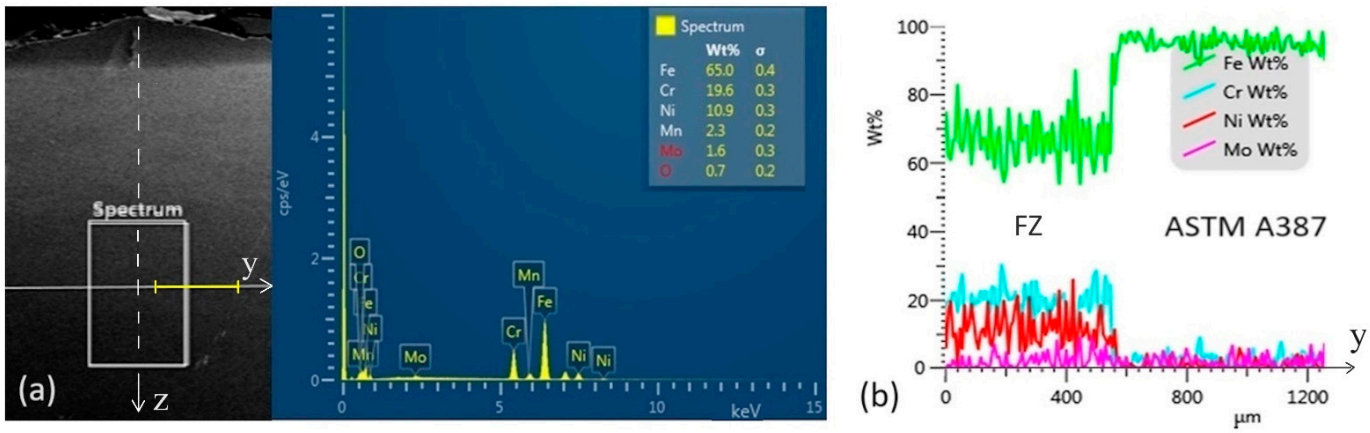

Figure 5. Results of SEM-EDS microanalysis: (**a**) area interested by the SEM-EDS measurements (delimited by the sides of the white rectangle, equal to 1.5 and 2.8 mm, respectively) with the resulting spectrum and average composition of the elements; (**b**) line scans taken along the yellow segment across the interface FZ/ASTM A387 shown in (**a**).

4. Discussion

The experimental values of Ni and Cr in Figure 5 are used to determine the equivalent compositions, while those of Mo and C, being too low to be reliable, can be obtained through a mass balance, taking into account the dilution ratios.

The mean value of the FZ area, measured by optical microscopy in three cross-sections (planes yz), results in A_{FZ} = 23.6 mm^2. Accordingly, the dilution ratios of the filler metal (d_F) and the base metals (d_B) are calculated from the following relationships:

$$d_F = A_F/A_{FZ} = 0.424 \quad d_B = (A_{FZ} - A_F)/A_{FZ} = 0.576 \tag{1}$$

With E_F being the mean concentration of a given element between the two filler metals, and E_B the weighted average value between the two base metals, the concentration in the FZ results in the following:

$$E_{FZ} = E_F \times d_F + E_B \times d_B \quad (2)$$

Using the values in Table 1, the concentrations of carbon and molybdenum in the FZ are obtained with Equation (2), resulting in C = 0.057%, and Mo = 1.49%. Then, the equivalent concentrations are calculated as follows:

$$Ni_{eq} = Ni\% + 35C\% = 10.9 + 35 \times 0.057 = 12.9\% \quad (3)$$

$$Cr_{eq} = Cr\% + Mo\% = 19.6 + 1.49 = 21.1\% \quad (4)$$

$$Cr_{eq}/Ni_{eq} = 21.1/12.9 = 1.63 \quad (5)$$

First, it can be noticed that the ratio Cr_{eq}/Ni_{eq} is in the range of 1.48–1.95, to which corresponds the presence of skeletal and/or lathy residual ferrite [11], as confirmed by the metallographic observations shown in Figure 4.

According to a consolidated procedure [17,19], the values of Cr_{eq} and Ni_{eq} allow us to identify a point on the WRC 1992 diagram, represented by the red circle in Figure 6. It is within the limit of the FA solidification mode with a residual ferrite percentage, or ferrite number (FN), not greater than 10%, which is useful to prevent hot cracking during solidification [7,14]. The solidification mode could vary with the cooling rate, which influences the ferrite–austenite transformations [20]; however, the analytical model experimentally fitted on the weld cross-section contour developed in [21], allowing cooling rate simulations, leads to the exclusion of variations in the expected values of FN for the welding conditions usually considered in LBW of 10 mm thick steel plates [22].

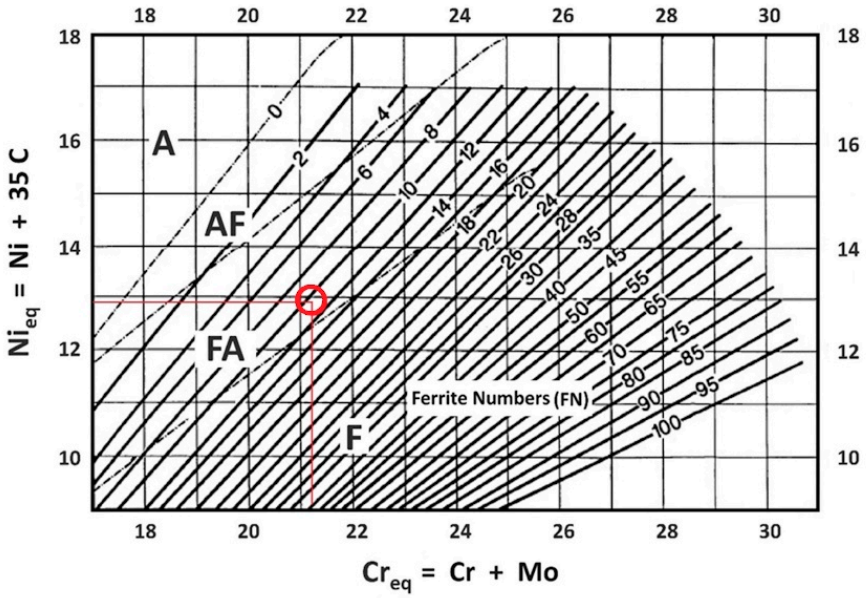

Figure 6. WRC 1992 diagram with indication of the FZ composition (red circle).

5. Conclusions

The choice of the LBW process parameters with two simultaneous laser beams and of the consumable insert composition allowed us to obtain a sound weld bead without serious misalignments or undercuts. The FZ showed a more regular profile if compared to that obtained with single laser welding. The satisfactory quality of the weld is confirmed by the experimental investigation carried out in the first stage of our research, which highlighted a microstructure characterized by an austenitic matrix with little residual ferrite (the best condition to prevent hot cracking). Compared to traditional arc welding, the considered

LBW process involves a smaller extension of the FZ, with a consequent reduction in the risk of distortions and residual stresses, resulting in an overall improvement in weldability of the dissimilar ASTM A387/AISI 304L steels. These results are encouraging for future developments aimed at the mechanical characterization of the welds, with the objective of a more in-depth evaluation of the weldability of thick dissimilar steel plates using two simultaneous laser beams.

Author Contributions: Conceptualization, F.G., S.M. and A.S.; methodology, F.G., S.M. and A.S.; investigation, F.G., S.M. and A.S.; data curation, F.G., S.M. and A.S.; writing—original draft preparation, F.G., S.M. and A.S.; writing—review and editing, F.G., S.M. and A.S.; visualization, F.G., S.M. and A.S.; supervision, F.G., S.M. and A.S. All authors have read and agreed to the published version of the manuscript.

Funding: This research received no external funding.

Data Availability Statement: The original contributions presented in the study are included in the article, further inquiries can be directed to the corresponding author/s.

Conflicts of Interest: The authors declare no conflicts of interest.

References

1. Dokme, F.; Kulekci, M.K.; Esme, U. Microstructural and mechanical characterization of dissimilar metal welding of Inconel 625 and AISI 316L. *Metals* **2018**, *8*, 797. [CrossRef]
2. Asadollahi, A.; Bahrami, A.; Shamanian, M. The effects of filler metal and butter layer on the microstructure and mechanical properties of API 5L X65/AISI 304L joint. *J. Mater. Res. Technol.* **2023**, *23*, 4148–4166. [CrossRef]
3. Sun, Y.L.; Obasi, G.; Hamelin, C.J.; Vasileiou, A.N.; Flinta, T.F.; Francis, J.A.; Smith, M.C. Characterization and modelling of tempering during multi-pass welding. *J. Mater. Process. Technol.* **2019**, *270*, 118–131. [CrossRef]
4. Sun, Y.L.; Hamelin, C.J.; Vasileiou, A.N.; Xiong, Q.; Flint, T.F.; Obasi, G.; Francis, J.A.; Smith, M.C. Effects of dilution on the hardness and residual stresses in multipass steel weldments. *Int. J. Press. Vessels Pip.* **2020**, *187*, 104154. [CrossRef]
5. Bahador, A.; Hamzah, E.; Mamat, M.F. Effect of filler metals on the mechanical properties of dissimilar welding of stainless steel 316L and carbon steel A516 GR 70. *J. Teknol.* **2015**, *75*, 61–65. [CrossRef]
6. Vargas, V.H.; Albiter, A.; Domínguez-Aguilar, M.A.; Altamirano, G.; Maldonado, C. Corrosion resistance of dissimilar GTA welds of pipeline steel and super duplex stainless steels. *Corros. J.* **2021**, *77*, 668–680. [CrossRef] [PubMed]
7. Weman, K. *Welding Processes Handbook*, 2nd ed.; Woodhead Publishing: Cambridge, UK, 2012; pp. 191–205.
8. Hoang, A.T.; Le, V.V.; Nguyen, A.X.; Nguyen, D.N. A study on the changes in microstructure and mechanical properties of multi-pass welding between 316 stainless steel and low-carbon steel. *J. Adv. Manuf. Technol.* **2018**, *12*, 25–40.
9. Boumerzoug, Z. A review: Welding by laser beam of dissimilar metals. *Asp. Min. Miner. Sci.* **2021**, *8*, 916–920. [CrossRef]
10. Zhang, M.; Chen, G.; Zhou, Y.; Liao, S. Optimization of deep penetration laser welding of thick stainless steel with a 10 kW fiber laser. *Mater. Des.* **2014**, *53*, 568–576. [CrossRef]
11. Nabavi, S.F.; Farshidianfar, A.; Dalir, H. A comprehensive review on recent laser beam welding process: Geometrical, metallurgical, and mechanical characteristic modeling. *Int. J. Adv. Manuf. Technol.* **2023**, *129*, 4781–4828. [CrossRef]
12. Scutelnicu, E.; Iordachescu, M.; Rusu, C.C.; Mihailescu, D.; Ocaña, J.L. Metallurgical and mechanical characterization of low carbon steel—Stainless steel dissimilar joints made by laser autogenous welding. *Metals* **2021**, *11*, 810. [CrossRef]
13. Hamada, A.; Khosravifard, A.; Ali, M.; Ghosh, S.; Jaskari, M.; Hietala, M.; Järvenpää, A.; Newishy, M. Micromechanical analysis and finite element modelling of laser-welded 5-mm-thick dissimilar joints between 316L stainless steel and low-alloyed ultra-high-strength steel. *Mater. Sci. Eng. A* **2023**, *882*, 145442. [CrossRef]
14. Yu, P.; Thompson, K.J.; McCarthy, J.; Kou, S. Microstructure evolution and solidification cracking in austenitic stainless steel. *Welds. Weld. J.* **2018**, *97*, 301s–314s. [CrossRef]
15. Zhou, C.; Dia, P.; Wu, H.; He, M.; Liu, X.; Chu, P.K. Effect of the ferrite morphology on hydrogen embrittlement of MAG welded 304 austenitic stainless steel. *Appl. Surf. Sci.* **2022**, *606*, 154866. [CrossRef]
16. Wang, Q.; Chen, S.; Rong, L. Properties of heavy-section AISI 316 stainless steel casting. *Met. Mater. Trans.* **2020**, *51*, 2998–3008. [CrossRef]
17. Missori, S.; Sili, A. Prediction of Weld Metal Microstructure in Laser Beam Weld Metal Clad Steel. *Metallurgist* **2018**, *62*, 84–92. [CrossRef]
18. *ISO 13919-1:2019*; Electron and Laser-Beam Welded Joints—Requirements and Recommendations on Quality Levels for Imperfections—Part 1: Steel, Nickel, Titanium and Their Alloys. ISO: Geneva, Switzerland, 2019.
19. Tandon, V.; Patil, A.P.; Kowshik, S. Impact of filler electrodes on welding properties of dissimilar welded 316L/201 austenitic stainless steels. *Eng. Proc.* **2023**, *59*, 90. [CrossRef]
20. Bunaziv, I.; Olden, V.; Akselsen, O.M. Metallurgical Aspects in the Welding of Clad Pipelines—A Global Outlook. *Appl. Sci.* **2019**, *9*, 3118. [CrossRef]

21. Giudice, F.; Missori, S.; Sili, A. Parameterized multipoint-line analytical modeling of a mobile heat source for thermal field prediction in laser beam welding. *Int. J. Adv. Manuf. Technol.* **2021**, *112*, 1339–1358. [CrossRef]
22. Giudice, F.; Sili, A. Weld metal microstructure prediction in laser beam welding of austenitic stainless steel. *Appl. Sci.* **2021**, *11*, 1463. [CrossRef]